Nuclear Science and Techniques (2025) 36:28
https://doi.org/10.1007/s41365-024-01599-8

A special core–shell material (Mxene@Ag@Phytate) to improve EVA composite fire safety, radiation cross-linking effect, and electromagnetic shielding

Si-Yi Xu[1,2] · Dan-Yi Li[1,2] · Wen-Rui Wang[1,2] · Lin Lin[1,2] · Ying Sun[1,2] · Ji-Hao Li[1,2] · Lin-Fan Li[1,2]

Received: 29 March 2024 / Revised: 26 April 2024 / Accepted: 4 May 2024 / Published online: 11 January 2025

Abstract
High-performance MXene-based polymer nanocomposites are well-suited for various industrial applications owing to their excellent mechanical, thermal, and other properties. However, the fabrication of flame-retardant polymer/MXene nanocomposites remains challenging owing to the limited flame-retardant properties of MXene itself. This study prepared a novel MXene@Ag@PA hybrid material via radiation modification and complexation reaction. This material was used to further enhance the key properties of ethylene-vinyl acetate (EVA), such as its mechanical properties, thermal conductivity, flame retardancy, and electromagnetic shielding. The addition of two parts of this hybrid material increased the thermal conductivity of EVA by 44.2% and reduced its peak exothermic rate during combustion by 30.1% compared with pure EVA. The material also significantly reduced smoke production and increased the residue content. In the X-band, the electromagnetic shielding effectiveness of the EVA composites reached 20 dB. Moreover, the MXene@Ag@PA hybrid material could be used to further enhance the mechanical properties of EVA composites under electron-beam irradiation. Thus, this study contributes to the development of MXene-based EVA advanced materials that are fire-safe, have high strength, and exhibit good electromagnetic shielding performance for various applications.

Keywords MXene@Ag@PA · Ethylene-vinyl acetate (EVA) · Flame retardancy · Electromagnetic shielding performance

1 Introduction

The widespread use of wearable electronic devices has significantly improved people's lives; however, it also presents challenges, including potential health risks from electromagnetic radiation and heat-related issues such as fires [1, 2]. To address these concerns, studies are actively searching for a multifunctional material with excellent fire resistance, heat dissipation properties, and ideal electromagnetic interference (EMI) shielding [3]. Although traditional metals have been considered as thermally conductive shielding films, they encounter issues such as corrosion, high density, and processing difficulties [4, 5]. Polymers such as ethylene-vinyl acetate copolymers (EVA) have gained attention because of their light weight, flexibility, low cost, and corrosion resistance. However, the challenge of interfacial incompatibility between the EVA matrix and conductive fillers has resulted in filler agglomeration, reducing both the electromagnetic shielding effectiveness and thermal conductivity [6]. Despite extensive efforts to address this issue, achieving an ideal electromagnetic shielding performance and thermal conductivity simultaneously remains a challenge. In addition, the flammability of EVA poses a risk of fire and thermal failure.

MXene, an emerging two-dimensional material, has attracted significant interest owing to its outstanding electromagnetic shielding and flame resistance properties [7]. Composed of metal titanium and carbon, the fundamental basic structure of MXene provides excellent electrical and thermal conductivity. This renders it ideal for addressing electromagnetic interference and fire-related issues [8, 9].

✉ Ji-Hao Li
lijihao@sinap.ac.cn

✉ Lin-Fan Li
lilinfan@sinap.ac.cn

[1] Shanghai Institute of Applied Physics, Chinese Academy of Sciences, Shanghai 201800, China

[2] University of Chinese Academy of Sciences, Beijing 100049, China

MXenes can be efficiently manufactured as shielding films to block or absorb electromagnetic radiation, thereby protecting electronic devices and communication systems from interference. Zhai et al. [10] dissolved waste cotton fabric (WCF) to prepare waste cotton cellulose aerogels and deposited MXene nanosheets onto them. Consequently, they obtained WCF/MXene composite aerogels with a high electromagnetic interference shielding effectiveness (EMI SE). The exceptional electromagnetic shielding performance of MXenes is crucial for mitigating electromagnetic pollution [11]. Moreover, MXene exhibits immense potential as a flame-resistant material for reducing fire risks and enhancing safety through its high thermal conductivity, rapid heat dissipation, and physical barrier properties that prevent flame penetration [12]. Despite the excellent performance of MXenes, challenges such as poor dispersion in polymers and susceptibility to oxidation at high temperatures or under fire conditions persist [13]. Researchers have actively sought solutions, including improved dispersion techniques and surface modifications, to enhance the stability of MXenes in practical applications [7–13].

Based on the aforementioned studies, it is evident that the current modification of MXenes primarily relies on chemical modifications [14, 15]. Although chemical modification has the potential to enhance material properties, it also has drawbacks such as environmental pollution, high costs, complex process control, generation of harmful byproducts, and limitations in material selection. The careful consideration and management of these issues are necessary when chemical modifications are used [16]. Radiation modification is a modern material processing technique that involves modifying and treating materials using various types of radiation sources, including electron beams, ultraviolet radiation, and ion beams. This technology has widespread applications in numerous industries, including medicine, food, materials science, and environmental protection. Radiation modification offers unique advantages including cleanliness, efficiency, and minimal environmental pollution. Compared to traditional heat treatment or chemical modification methods, radiation modification typically requires fewer processing steps, reducing the time and resource wastage during the production process [17]. In addition, radiation modification exerts a minimal environmental impact. In contrast to certain chemical processing methods, it does not generate harmful chemical byproducts during the treatment process, thereby lowering the risks to personnel and environmental health. Han [18] et al. utilized radiation technology to develop a straightforward two-step method for preparing silver (Ag) nanocluster composite materials. First, they grafted polyacrylic acid (PAA) chains onto the surfaces of polyethylene (PE) membranes to serve as templates (PE-g-PAA). Subsequently, through in situ reduction of Ag ions on the surface of the template material, Ag nanocluster composite materials (AgNCs@PE-g-PAA) were formed. This composite material can function as a fluorescent test paper, enabling visual detection of Cr^{3+} ions.

To enhance the dispersion of MXene in EVA and create multifunctional materials, this study employed $AgNO_3$ as a precursor and a radiation reduction method to synthesize Ag nanoparticles modified MXene (MXene@Ag). Subsequently, MXene@Ag was coated with phytic acid (PA) to prepare a novel core–shell structured material known as MXene@Ag@PA hybrid. The MXene@Ag@PA hybrid material was then incorporated into EVA through melt blending to create multifunctional EVA flame-retardant composite materials. This study investigated flame retardancy, mechanical properties, radiation resistance, and electromagnetic shielding performance. In addition, the combustion residues were analyzed to explore the flame-retardant mechanism of MXene@Ag@PA hybrid material.

2 Experimental section

2.1 Materials

Ti_3AlC_2 (MAX, 98 wt%, 400 mesh) was purchased from Foshan Xinene Technology Co., Ltd. Lithium fluoride (LiF, ≥99%, CP), silver nitrate ($AgNO_3$, ≥99.8%, AR), and anhydrous ethanol (EtOH, AR) were purchased from Shanghai Aladdin Biochemical Technology Co., Ltd. Hydrochloric acid (HCl, 36% –38%, AR) was provided by Tianjin Komiou Chemical Reagent Co., Ltd. EVA (2803, containing 28% vinyl acetate) was purchased from Arkema (France). Phytic acid (70 wt% in H_2O) was purchased from Shanghai Zhanyun Chemical Co., Ltd.

2.2 Fabrication of exfoliated MXene (e-MXene)

MXene was synthesized according to a previous study [19] using the following method. First, 1 g of LiF was slowly added to hydrochloric acid solution (20 ml, 9 g/mol) to form a homogeneous solution. Then, 1.0 g MAX powder was slowly added to the above solution within 30 in. The mixture was then continuously stirred at 40 °C for 48 h after the aluminum layer was removed. MXene was obtained after centrifugation (5000 rad/min for 5 in) and washed with deionized water until the pH was >6. The exfoliated MXene was further exfoliated via ultrasonication for 60 in and centrifuged at 3500 rad/min for 30 in to obtain a uniformly exfoliated MXene suspension. Finally, the exfoliated MXene powder was obtained by freeze drying.

2.3 Fabrication of MXene@Ag

Thereafter, 0.5 g of exfoliated MXene powder and 0.5 g of $AgNO_3$ were added to 250 ml of deionized water and stirred for 2 h via sonication. Similarly, 250 ml ethanol was added to the solution under mechanical stirring and sonication. The prepared exfoliated MXene suspension was evacuated for 15 min and then passed through nitrogen for 15 min to remove oxygen. It was then irradiated with a cobalt source (^{60}Co) with an absorbed dose of 30 kGy and a dose rate of 2.5 kGy h^{-1}. Finally, the produced MXene@Ag nanostructure was collected via vacuum filtration, washed with deionized water, and placed in a vacuum oven at 60 °C for drying for 24 h.

2.4 Fabrication of MXene@Ag@PA

Then, 10 ml of PA was poured into 90 ml of deionized water to prepare a 10% concentration phytic acid solution. Further, 0.2 g of MXene@Ag was added to this phytic acid solution and stirred using a magnet for 2 h. After the completion of the reaction, the sample was filtered, washed, and vacuum-dried at 60 °C to obtain MXene@Ag @PA. The experimental steps are shown in Fig. 1.

2.5 Fabrication of EVA/MXene@Ag@PA composites

The EVA/MXene@Ag@PA0.5 composites were prepared by blending. First, 99.5 g EVA resin and 0.5 g MXene@Ag@PA were blended using a small mixer. Subsequently, the composite materials were kept under the conditions of 18 MPa and 175 °C for 5 min to form plane sheets. The composites were named as EVA/MXene@Ag@PA1.0, EVA/MXene@Ag@PA1.5, and EVA/MXene@Ag@PA2.0 by adding 1.0 g of MXene@Ag@PA, 1.5 g of MXene@Ag@PA, and 2.0 g of MXene@Ag@PA instead of EVA, respectively. Further, pure EVA was used for comparison.

2.6 Characterization

The Fourier transform infrared (FTIR) spectra of the samples were recorded using a Bruker Vector 33 spectrometer (Germany) with a resolution of 4 cm^{-1} over 32 scans in the range of 4000 – 400 cm^{-1}. X-ray diffractions (XRD) measurements were performed at a scan speed of 0.01°/s in the range of 5°–80° using a Bruker D8-Advance with Cu Kα radiation at 1.5418 angstrom. Scanning electron microscopy and energy-dispersive X-ray spectrometry (SEM-EDS) were employed to observe the morphologies of the samples with a SEM (TM4000, Japan) at an accelerating voltage of 15 kV. Thermogravimetric analysis (TGA) was performed using a thermogravimetric analyzer

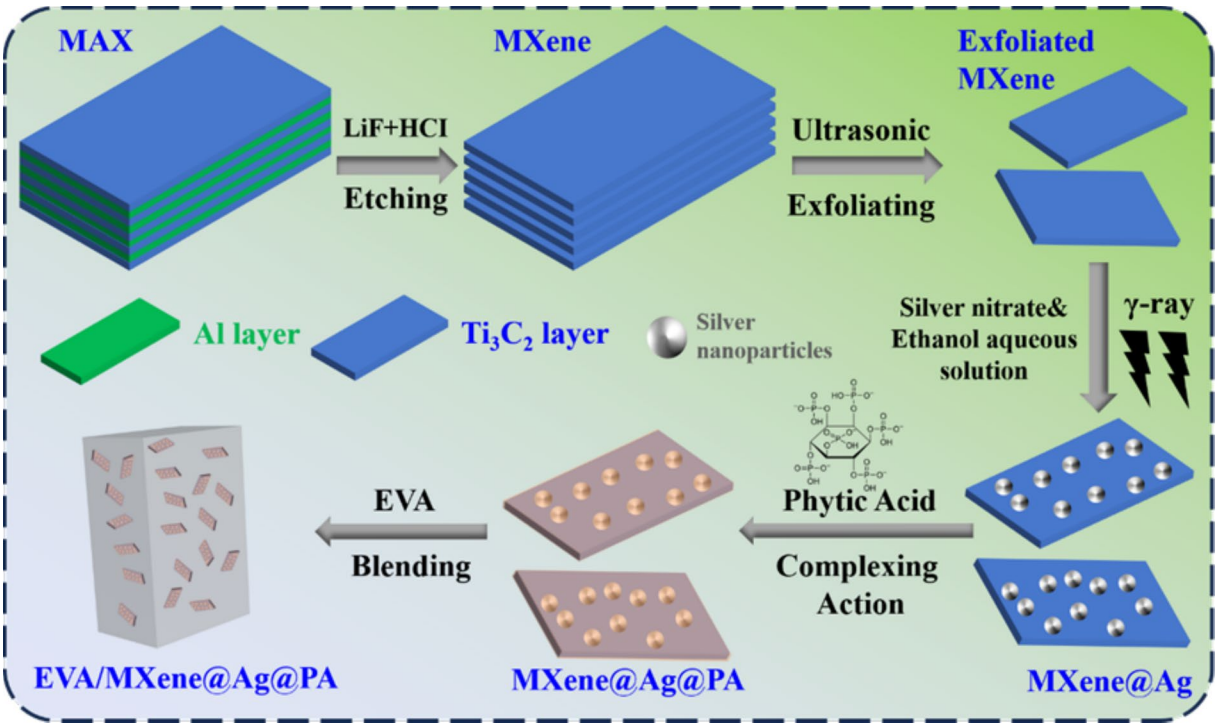

Fig. 1 (Color online) Preparation of MXene@Ag@PA

(STA449C, NETZSCH, Germany) at a heating rate of 15 °C min^{-1} under a nitrogen atmosphere. A cone calorimeter test (CCT) was conducted on an FTT cone calorimeter according to ISO 5660 at a heat flux of 35 kW m^{-2} (sample size:100 mm × 10 mm × 3 mm). The mechanical performance was tested using a WZY-240 (Chengde Hengtong Testing Instruments Co. Ltd) universal machine at a constant rate of 200 mm min^{-1}, and the samples were cut into dumbbells of 4 mm thickness according to GB/T 1040-2006. The same samples were tested at least five times, and the average results were obtained. Mechanical performance testing was conducted following electron-beam irradiation. The mechanical properties of each sample were tested after irradiation with electron beams of different absorbed doses. The absorbed doses considered were 100 kGy, 200 kGy, 300 kGy, 400 kGy, and 500 kGy. Thermal conductivity (TC) was measured employing the transient hot wire method using a TC3000E TC meter. The length, width, and height of the solid test sample were not less than 25 mm × 25 mm × 3 mm; therefore, the upper and lower sides of the samples on both sides of the sensor were kept flat. An AV3629 vector network analyzer was used to test the electromagnetic shielding performance of EVA and its composite. *S* and electromagnetic parameters were measured using the coaxial airline method. The test band was the X-band (8.2 GHz to 12.4 GHz). Raman spectra were measured using a LabRAM spectrometer (DilorSA, France) with a 532 nm argon laser line.

3 Results and discussion

3.1 Characterization of MXene@Ag@PA

Infrared (IR) and XRD analyses of the synthesized product confirmed the successful synthesis of MXene@Ag@PA. As shown in Fig. 2a, characteristic peaks for pure MXene were observed at 3373 cm^{-1} and 1384 cm^{-1}, corresponding to the –OH and C–F functional groups, respectively. These chemical bonds represent new bonds formed on the MXene surfaces during delamination. After introducing PA to create the MXene@Ag@PA hybrid material, two new characteristic peaks appeared in the infrared spectrum at 1215 cm^{-1} (P-O) and 1157 cm^{-1}(P=O), indicating that PA might have undergone complexation reactions with either C-Ti or Ag in MXene during the reaction process [20, 21]. Furthermore, in the XRD curve (Fig. 2b), a distinct peak was observed at approximately 6.5° for exfoliated MXene.

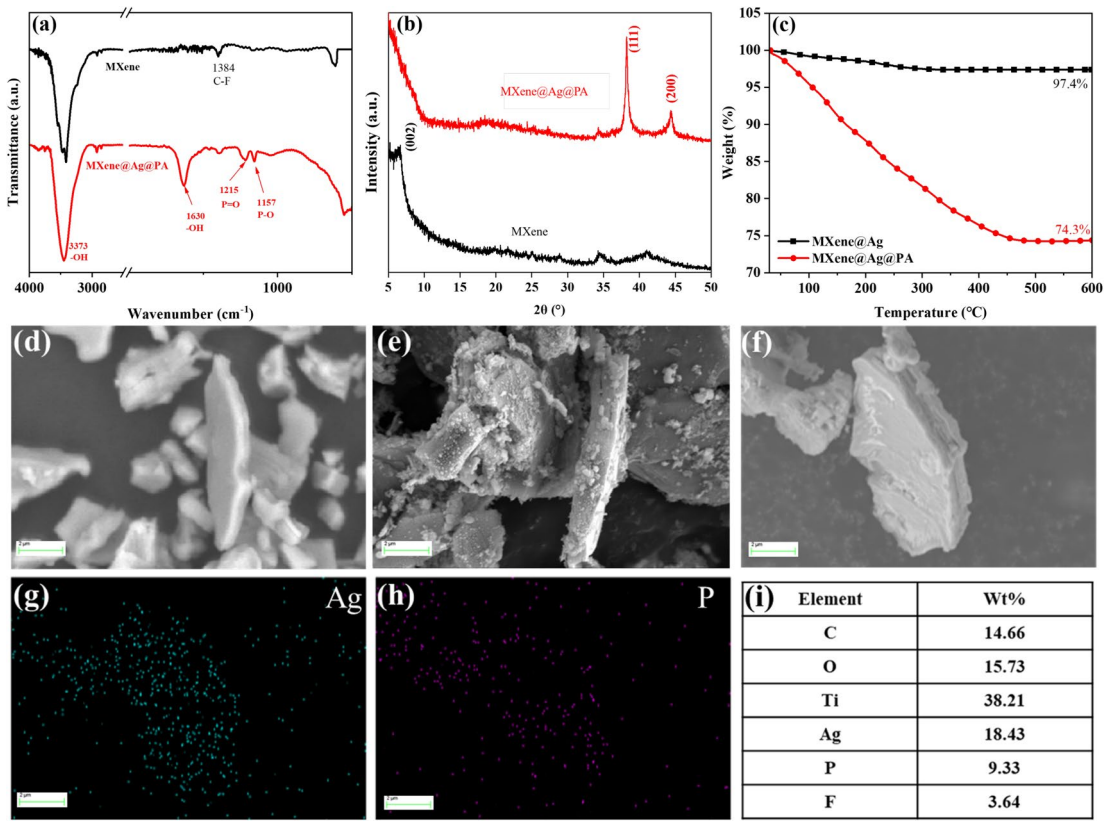

Element	Wt%
C	14.66
O	15.73
Ti	38.21
Ag	18.43
P	9.33
F	3.64

Fig. 2 (Color online) FTIR (**a**), XRD (**b**), and TG (**c**) of MXene and MXene@Ag@PA; SEM images of MXene (**d**), MXene@Ag (**e**), and MXene@Ag@PA (**f**); and EDS mapping of Ag element (**g**), P element (**h**), and EDS element content (**i**) of MXene@Ag@PA

This was attributed to the leftward shift of the characteristic peak corresponding to the (002) crystal plane of MXene, indicating the successful exfoliation of MXene using LiF and HCl. For MXene@Ag@PA, XRD revealed two typical crystal planes, (111) and (200), for Ag nanoparticles at approximately 38.9° and 43.4°, respectively. This implied the successful formation of Ag nanoparticles under the action of radiation reduction [22]. Interestingly, the (002) crystal plane of the exfoliated MXene disappeared after coating with PA, which may be attributed to the formation of a protective layer through complexation with PA on the MXene surface, resulting in shielding effects.

Figure 2c shows the thermal stability change curves of the MXene@Ag and PA-modified MXene@Ag@PA hybrid materials. As evident, the thermal degradation of the MXene@Ag hybrid material gradually decreased as the temperature increased. The residue content was 600 °C when the temperature reached 97.4% . The decrease in the residue content at high temperatures may be attributed to the removal of functional groups containing O and F from the surface of the MXene@Ag hybrid material. Interestingly, after modifying MXene@Ag hybrid material with PA, the thermal stability of MXene@Ag@PA hybrid material significantly decreased [23, 24]. The initial thermal decomposition temperature ($T_{5\%}$) of this material decreased to 149.2 °C. Furthermore, as the temperature increased, the residue content decreased significantly, particularly when the heating temperature reached 600 °C, where the residue content decreased to 74.3%. Compared to MXene@Ag hybrid material, this indicated a reduction of 23.1%. Thus, when the MXene@Ag hybrid material was coated with PA, the PA loading was approximately 23.1%.

SEM-EDS analysis provided a more intuitive insight into the morphological changes and elemental distribution before and after the PA coating of MXene@Ag. From Fig. 2e, compared to pure MXene (Fig. 2d), the surface of exfoliated MXene@Ag, under the influence of radiation reduction, generated numerous small nanoparticles, all of which were Ag nanoparticles. The surface of MXene@Ag@PA obtained after coating the MXene@Ag hybrid material with PA was subjected to significant changes (Fig. 2e). This was primarily evident from the significant reduction in the number of nanoparticles originally present on the surface, rendering the surface relatively smooth [25]. Therefore, PA effectively adhered to the shell structure on the surface of MXene@Ag hybrid material. To further confirm the presence of Ag nanoparticles inside MXene@Ag@PA hybrid material, EDS was used for elemental analysis, and the elemental distribution maps are shown in Fig. 2f-h. The elemental compositions shown in Fig. 2i clearly indicate the presence of the key elements P and Ag, which were generated during the synthesis process. This confirmed the successful synthesis of MXene@Ag@PA hybrid material.

3.2 Characterization of EVA and its composites

The impact of the incorporation of the MXene@Ag @ PA hybrid material on the internal structure of EVA was observed and analyzed using SEM. As in Fig. 3a, the cross section of pure EVA after fracture appeared relatively smooth, with no apparent cracks. When a small amount of the MXene@Ag@PA hybrid material was added, small particles appeared in the cross section of the EVA composite material, and these particles were all derived from the

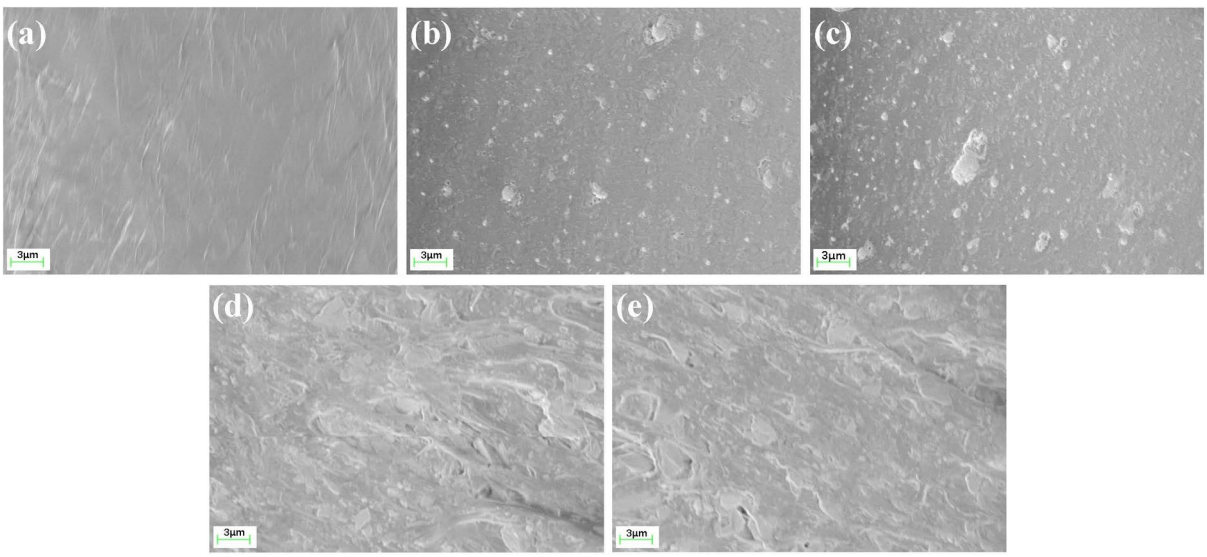

Fig. 3 (Color online) SEM images of the sections of EVA and its composites: EVA (**a**), EVA/MXene@Ag@PA0.5 (**b**), EVA/MXene@Ag@PA1.0 (**c**), EVA/MXene@Ag@PA1.5 (**d**), and EVA/MXene@Ag@PA2.0 (**e**)

exfoliated MXene@Ag@PA hybrid material (Fig. 3b, c). Interestingly, when the amount of the MXene@Ag@PA hybrid material was less than one part, the fracture surface of the EVA composite material remained relatively smooth without voids or cracks [26]. Thus, the addition of a small amount of MXene@Ag@PA hybrid material had a relatively minor impact on the internal structure of EVA. Furthermore, because most MXene@Ag@PA hybrid material particles are smaller than 1 μm, this may result in a reinforcing effect owing to the nanoscale effect. Thus, increasing the content of the MXene@Ag@PA hybrid material negatively affected the internal structure of the EVA composite material, and this effect can be observed more directly in Figs. 3d and e. These two images show that the addition of a large amount of the MXene@Ag@PA hybrid material tended to result in aggregation, thereby reducing the compatibility between the MXene@Ag@PA hybrid material and EVA, and increasing the number of pores and voids [27]. This reduction in the integrity of the cross section of the EVA composite material renders it challenging for the aggregated MXene@Ag@PA hybrid material to serve as a physical cross-linking point, which may exert detrimental effects on the mechanical properties.

3.3 Key properties of EVA and its composites

TGA was conducted to analyze the thermal stability of EVA and its composite materials. Figure 4a shows that the initial thermal decomposition temperature ($T_{5\%}$) of pure EVA was 350.1 °C. With the continuous addition of the MXene@Ag@PA hybrid material, the $T_{5\%}$ of the EVA composite material increased slightly, possibly because of the decomposition of PA in the MXene@Ag@PA hybrid material. Furthermore, as shown in Fig. 4b, two decomposition peaks (T_{m1} and T_{m2}) were observed in the curves corresponding to each sample. These two peaks corresponded to the degradation of the EVA side and main chains, respectively. However, a comparison revealed that the maximum decomposition rate temperatures corresponding to both peaks in EVA composite materials containing MXene@Ag@PA hybrid material were lower than that of pure EVA. Therefore, the presence of the MXene@Ag@PA hybrid material promoted

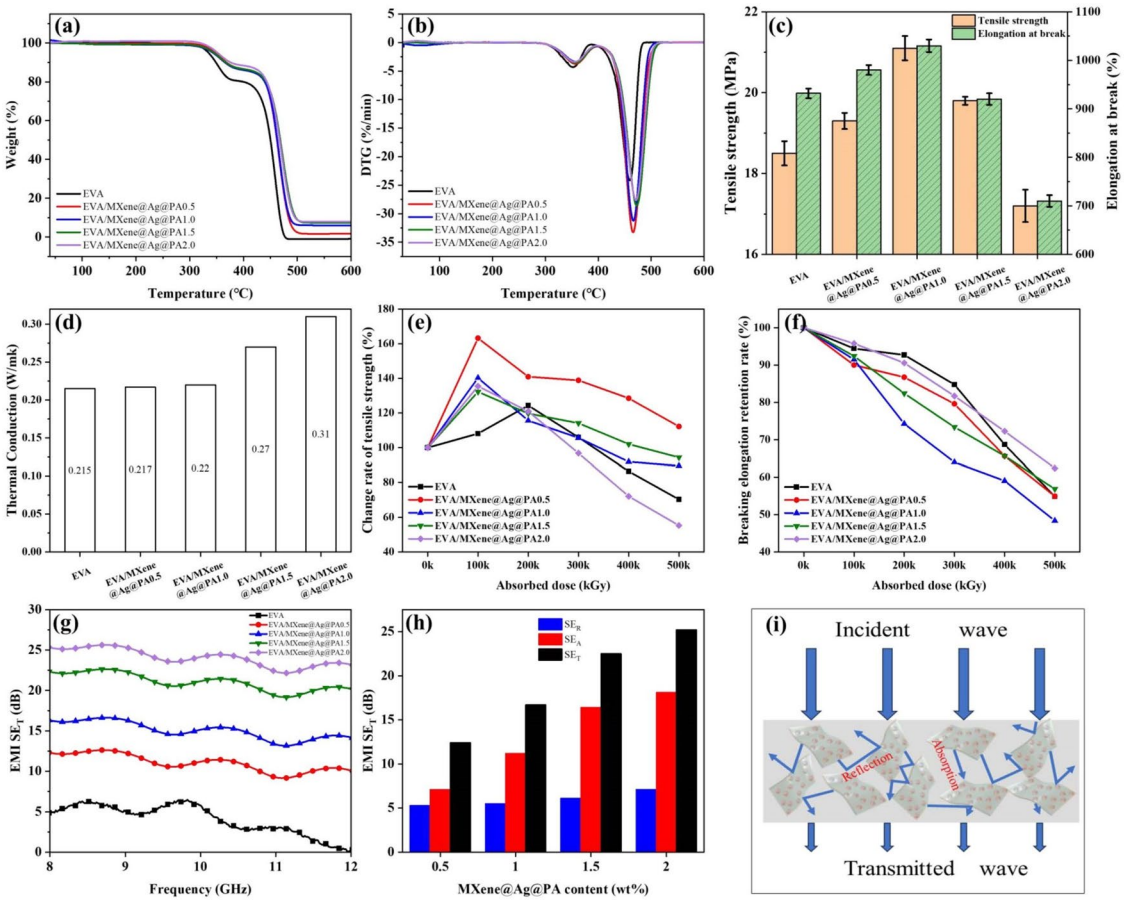

Fig. 4 (Color online) TGA (**a**), DTG (**b**), mechanical property (**c**), thermal conduction (**d**), retention rate of mechanical properties before and after irradiation (**e** represents elongation at break; **f** represents tensile strength), EMI SE in the X-band (**g**), and SET, SEA, and SER at 8.8 GHz (**h**) of EVA and its composites; and EMI shielding mechanism (**i**)

the decomposition and carbonization of EVA. The catalytic carbonization effect of the MXene@Ag@PA hybrid material exerted a positive impact on the residue content of the EVA composite materials [28, 29]. Therefore, from Fig. 4a at 600 °C, it can be observed that the addition of more MXene@Ag@PA hybrid material effectively increased the residue content when the EVA composite materials were completely thermally decomposed. Moreover, when the addition of MXene@Ag@PA hybrid material was 1.5 or 2 by parts, a relatively small change in the residue content of EVA composite materials was observed. Therefore, the excessive addition of MXene@Ag@PA hybrid material limited the catalytic carbonization effects.

Macroscopic performance testing was conducted to explore the effect of the addition of the MXene@Ag@PA hybrid material on the mechanical properties and thermal conductivity of the EVA composite materials. Figure 4c shows that the tensile strength and elongation at break of pure EVA were 18.5 MPa and 933% , respectively. When 1 part of the MXene@Ag@PA hybrid material was added, the performance of the EVA composite material improved significantly, and the tensile strength and elongation at break increased to 21.1 MPa and 1070% , respectively. This indicated improvements of 14.1% and 14.7% compared to pure EVA [30]. Thus, the addition of an appropriate amount of MXene@Ag@PA hybrid material can enhance the mechanical properties of EVA, possibly because of the good compatibility between MXene@Ag@PA hybrid material and EVA and the nanoreinforcement effect of MXene@Ag@PA hybrid material's two-dimensional structure. However, further increasing the content of MXene@Ag@PA hybrid material reduced the mechanical properties of the EVA composite material, which may be caused by the agglomeration of MXene@Ag@PA hybrid material, which can also be observed in SEM images.

Furthermore, as the content of MXene@Ag@PA hybrid material increased, the thermal conductivity of the EVA composite material continued to increase (Fig. 4d). When the MXene@Ag@PA hybrid material reached 2 parts, the thermal conductivity reached 0.31 W/(m · K), which is an improvement of 44.2% compared to pure EVA. This is because the presence of a large amount of MXene@Ag@PA hybrid material can create thermal conduction pathways within the EVA, thereby enhancing the speed of heat transfer and thus promoting an increase in thermal conductivity.

Figure 4e-f shows the influence of different electron-beam absorbed doses on the retention of the mechanical properties of EVA and its composite materials. Based on the trends in the curves shown in Fig. 4e, it can be observed that when the absorbed dose was below 200 kGy, the tensile strength retention rate of pure EVA increased. However, it decreased as the absorbed dose continued to increase. Thus, pure EVA is primarily radiation cross-linked when the absorbed dose is below 200 kGy, whereas absorbed doses higher than 200 kGy begin to negatively affect pure EVA through radiation degradation. Interestingly, the addition of the MXene@Ag@PA hybrid material did not significantly affect the tensile strength retention rate of the EVA composite, effectively reducing the absorbed dose required for radiation cross-linking in the composite. According to the experimental results, when the absorbed dose reached 100 kGy, the tensile strength retention rate of EVA composite material with the addition of 0.5 parts of MXene@Ag@PA hybrid material increased to 164% . A further increase in the absorbed dose exerted a negative impact. Therefore, the MXene@Ag@PA hybrid material functioned as a radiation sensitizer. The graph shows that the addition of more MXene@Ag@PA hybrid material, while not achieving the desired enhancement in the tensile strength retention rate, could still increase it to approximately 130–140% . This demonstrated the role of the MXene@Ag@PA hybrid material in promoting polymer radiation cross-linking. This may be because high-energy electron beams break the P-OH bonds contained in the PA in MXene@Ag@PA, generating more free radicals that promote cross-linking with polymer free radicals. Moreover, under the influence of high-energy radiation, MXene and Ag may release more heat, further promoting cross-linking of the EVA composite material. However, excessive addition of the MXene@Ag@PA hybrid material may hinder the cross-linking between free radicals on the EVA molecular chain, thus negatively affecting the radiation cross-linking efficiency [20]. Furthermore, the significant cross-linking effect of MXene@Ag@PA hybrid material on the EVA composite material at low absorbed doses inhibited the movement of the EVA molecular chains, thereby reducing the elongation at break retention rate. Excessive absorbed doses can break the EVA molecular chains, further reducing the elongation at the break retention rate, as shown in Fig. 4e.

The different MXene@Ag @PA contents affected the electromagnetic shielding effectiveness (EMI SET) of the EVA composite materials. As shown in Fig. 4g, pure EVA has a relatively low EMI SET value in the X-band. When the addition of MXene@Ag@PA reached 0.5 by parts, the maximum EMI SET value increased to 12.5 dB, indicating that the shielding effectiveness was significantly improved [31]. When the addition of MXene@Ag@PA reached 1.0 by parts, the EMI SET curve consistently exceeded 20 dB in the X-band, implying that the output signal's energy was only one-tenth of the input signal's energy. During shielding and signal processing, 20 dB attenuation was considered to exert a significant suppression effect [32]. A further increase in the amount of MXene@Ag@PA allowed the EMI SET of the EVA composite material to reach 25.2 dB at 8.8 GHz. To investigate the EMI shielding mechanism of the EVA/MXene@Ag@PA composite, the total EMI shielding

effectiveness (SET), absorption SE (SEA), and reflection SE (SER) were calculated at 8.8 GHz, as shown in Fig. 4h. The SEA of the EVA/MXene@Ag@PA composite was significantly higher than the SER. For example, in EVA/MXene@Ag@PA 2.0, the SET, SEA, and SER were 25.2 dB, 18.1 dB, and 7.1 dB, respectively. Further, the percentage of SEA in the SET was 71.8% , indicating that microwave absorption played a dominant role in the shielding process, reducing the secondary EMI pollution generated by microwave reflection. When electromagnetic microwaves encounter the surface of the EVA composite material, most pass through the EVA layer, with only a small portion being reflected. Owing to the presence of MXene@Ag@PA, the incident electromagnetic microwaves are reflected at the MXene@Ag@PA-EVA interface. The incident electromagnetic microwaves are captured, absorbed, or dissipated as heat within the material. Subsequently, the remaining electromagnetic microwaves are consumed through multiple reflections and alternating structures between the conductive MXene layers (Fig. 4i) [12].

3.4 Burning behaviors of EVA and its composites

Through CCT, the thermal behavior, smoke production, and residue content during the simulated combustion of EVA and its composites were analyzed to comprehensively assess the flame-retardant performance of the EVA composites. As shown in Fig. 5a, the peak heat release rate (pHRR) of pure EVA was 688.2 kW m^{-2}, whereas the EVA composite with the addition of 0.5 parts of MXene@Ag@PA hybrid material exhibited a pHRR of 687.7 kW m^{-2}. Thus, a relatively minor difference was observed between the two. This suggests that a small amount of MXene@Ag@PA hybrid material cannot effectively suppress the maximum heat release from the EVA composite during combustion [33]. This limited effect can be attributed to the challenge of achieving ideal catalytic

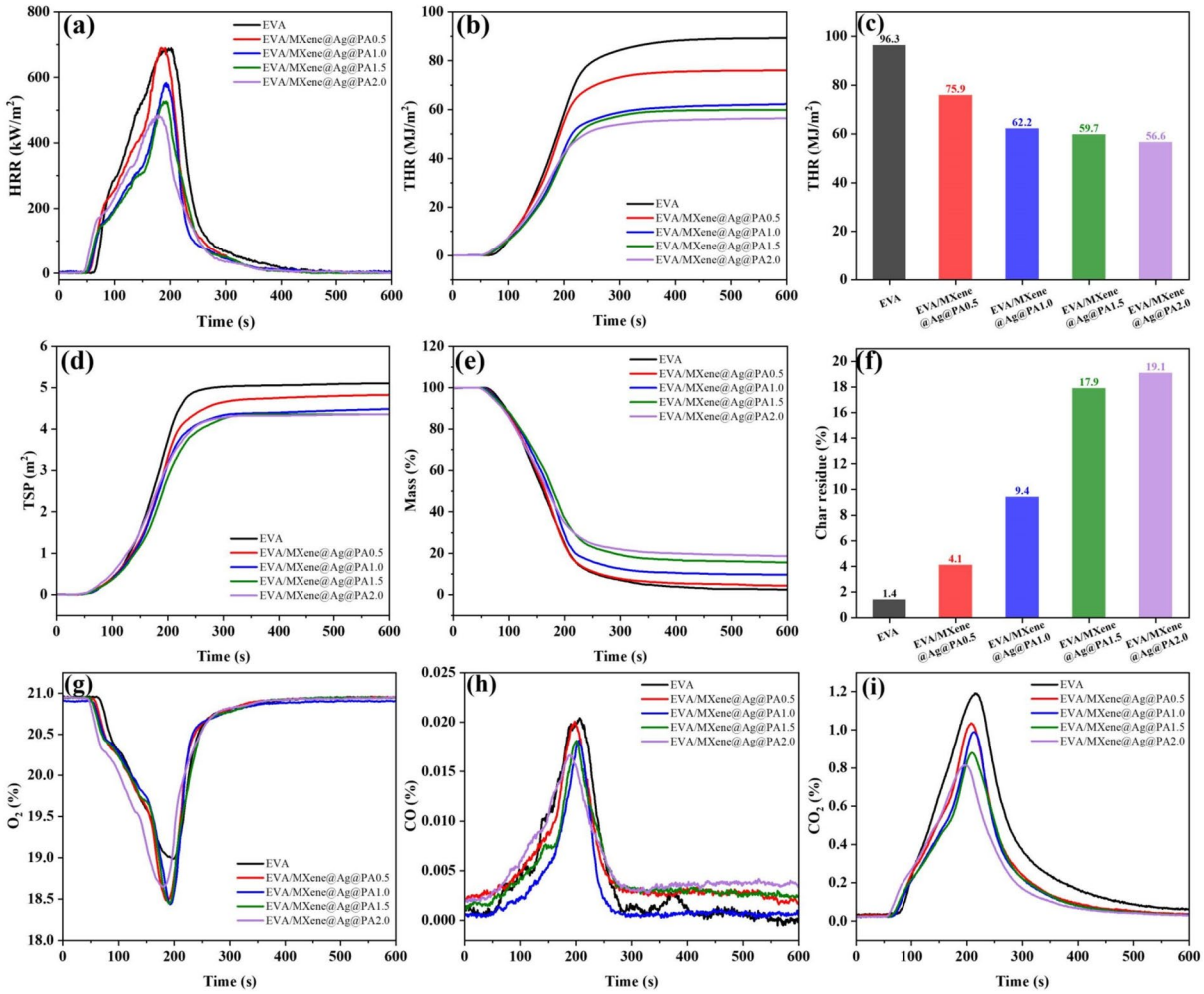

Fig. 5 (Color online) HRR (**a**), THR (**b**,**c**), TSP (**d**), mass (**e**), char residue (**f**), O_2 (**g**), and CO (**h**), an CO_2 (**i**) content of EVA and its composites during CCT

char formation with a small quantity of MXene@Ag@PA and the difficulty of forming a physical barrier on the surface of the EVA composite during combustion. Consequently, flames and heat can readily penetrate, thereby accelerating the decomposition of combustibles and resulting in no significant change in pHRR. However, when the quantity of MXene@Ag@PA hybrid material exceeded 1 part, a notable reduction in the pHRR of the EVA composite was observed. Upon adding two parts of MXene@Ag@PA hybrid material, the pHRR decreased to 481.2 kW m^{-2}, resulting in a 30.1% reduction compared with pure EVA. Therefore, during the most intense burning of the EVA composite, less heat was released, which reduced the likelihood of igniting nearby combustibles.

Figure 5b and c illustrates the total heat release (THR) of EVA and its composite materials during complete combustion. Pure EVA exhibited a THR of 96.3 MJ m^{-2}, whereas the addition of 0.5 parts of MXene@Ag@PA hybrid material, while not significantly affecting pHRR, reduced THR to 75.9 MJ m^{-2}. Thus, the MXene@Ag@PA hybrid material retained its catalytic charring effect, albeit to a limited extent. However, when the quantity of the MXene@Ag@PA hybrid material reached two parts, the THR decreased to 56.6 MJ m^{-2}, which was a 41.2% reduction compared with pure EVA [34]. This significant reduction can be attributed to the abundance of catalytic MXene and Ag within MXene@Ag@PA hybrid material and the dehydrative carbonization capability of PA.

The investigation of smoke production by EVA and its composite materials is also of significant importance. This is because excessive smoke generated during combustion can pose a threat to human life when inhaled. As shown in Fig. 5c, pure EVA exhibited higher values for both the peak smoke release rate and total smoke production (TSP) than the other samples. The addition of the MXene@Ag@PA hybrid material effectively reduced smoke release. When the quantity of the MXene@Ag@PA hybrid material reached two parts, the TSP decreased to 4.3 m^2, representing a 28.3% reduction compared with pure EVA (Fig. 5d) [35]. Moreover, the increase in residue content further facilitated the reduction in TSP. As shown in Fig. 5e and f, the addition of MXene@Ag@PA hybrid material effectively reduced the mass-loss rate of the EVA composite materials during combustion. Consequently, the residue content increased. When two parts of MXene@Ag@PA hybrid material were added, the residue content of the EVA composite material after complete combustion reached 19.1% , whereas that of pure EVA was only 1.4%. The significant increase in the residue content confirms that more smoke molecules could be transformed into stable carbon layers without being released into air. This phenomenon is attributed to the excellent catalytic and dehydrative carbonization capabilities of MXene@Ag@PA hybrid material.

The changes in oxygen consumption and carbon monoxide (CO) and carbon dioxide (CO_2) emissions in EVA and its composite materials during combustion provided a more intuitive analysis of the flame-retardant effect of MXene@Ag@PA hybrid materials. Figure 5g shows that pure EVA consumed the most oxygen at a combustion time of 200 s, thereby reducing the oxygen concentration to approximately 19.1%. In contrast, the samples containing the MXene@Ag@PA hybrid material consumed more oxygen during combustion, indicating that more oxygen was involved in the combustion reaction. The fate of this oxygen, whether it eventually transforms into CO and CO_2 or forms other substances, is illustrated by the changes in the CO and CO_2 contents presented in Fig. 5h and i, respectively. The patterns in the figures suggest that the MXene@Ag@PA hybrid material did not convert O_2 into gases but rather partially inhibited the release of CO and CO_2 [36]. In particular, when the quantity of the MXene@Ag@PA hybrid material was 2 parts, the peak concentration of CO decreased from 0.021% exhibited by pure EVA to 0.017%. Whereas, the peak concentration of CO_2 decreased from 1.2% to 0.8%. This phenomenon demonstrated that the catalytic effect of the MXene@Ag@PA hybrid material may promote the reaction of O_2 with combustibles in the EVA composite material, thus forming less readily released and more stable substances such as residual carbon. Consequently, the emission of the toxic CO gas is reduced [37].

Figure 6a–d provides microscopic images of the residual structure formed after the complete combustion of the EVA composite. The surfaces or interiors of the residues of the individual samples showed the appearance of lamellar materials, and the amount of these lamellar materials increased with the addition of the MXene@Ag@PA hybrid material. This suggests that these plate-like substances are likely residual structures that remain after combustion and decomposition of the MXene@Ag@PA hybrid material [38]. The presence of these substances promoted the formation of residual materials in the EVA composites and made the structure of the residual carbon denser and more stable. Consequently, this effectively inhibited the penetration of external flames and combustible gases and prevented the decomposition of internal combustibles.

Further analysis of the residual carbon could effectively determine the extent of catalytic carbonization of the MXene@Ag@PA hybrid material during the combustion of the EVA composite materials. Raman spectroscopy was used to characterize the structure of the residual material, and the results are shown in Fig. 6e–h. As evident, two primary characteristic peaks were observed, located around 1300 cm^{-1} – 1400 cm^{-1} (D-band) and near 1600 cm^{-1} (G-band). The ratio of the intensities of the D-band and G-bands determined which component, amorphous or graphitic, dominated the residual carbon [39]. In the Raman

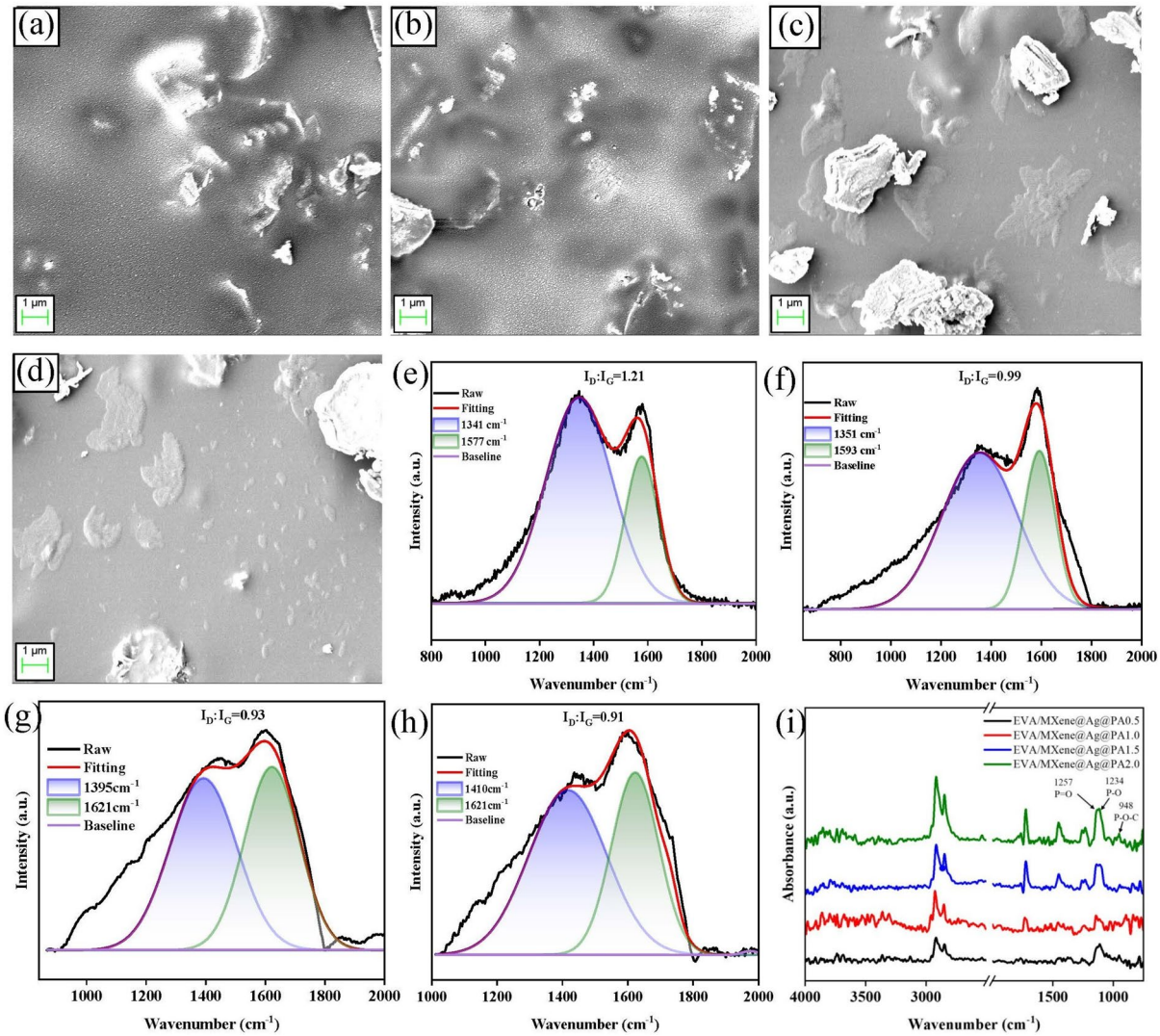

Fig. 6 (Color online) SEM images (**a**-**d**), Raman spectra (**e**-**h**), and FTIR (**i**) of the external char residues for EVA composites; EVA/MXene@Ag@PA0.5 (**a**,**e**), EVA/MXene@Ag@PA1.0 (**b**,**f**), EVA/MXene@Ag@PA1.5 (**c**,**g**), and /MXene@Ag@PA2.0 (**d**,**h**)

spectra, the I_D:I_G value for the EVA/MXene@Ag@PA0.5, composite material was 1.21. As the content of MXene@Ag@PA hybrid material increased, the ratio gradually decreased, indicating an increasing graphitic content in the residual material. When the amount of MXene@Ag@PA hybrid material reached 2 parts, I_D:I_G decreased to 0.91. Therefore, the presence of MXene@Ag@PA effectively enhanced the graphitization of the residual material and improved the density and stability of the carbon layer.

The organic components of the combustion residues of the EVA composites were analyzed using IR spectroscopy. Figure 6i shows that in the residues formed by the complete combustion of the sample with only 0.5 parts of MXene@Ag@PA hybrid material, only the C-H symmetric and asymmetric stretching vibration peaks at 2912 cm^{-1} and 2840 cm^{-1} were visible. This was attributed to the molecular chains remaining after EVA combustion. In addition, double peaks were observed at 1257 cm^{-1} and 1234 cm^{-1}, which were characteristic of the P=O and P-O bonds in MXene@Ag@PA hybrid material, respectively. Interestingly, as the content of the MXene@Ag@PA hybrid material increased, the intensities of the P=O and P-O characteristic peaks also increased. A new characteristic peak appeared at 948 cm^{-1}, which corresponded to the newly formed P-O-C bond during combustion. Therefore, the MXene@Ag@PA hybrid material reacted with the EVA molecular chains during combustion to form new chemical bonds, thereby increasing the stability of the carbon layer. Furthermore, in the figure, new peaks appeared at 1448 cm^{-1} and 1712 cm^{-1} as the content of MXene@Ag@PA hybrid material increased. These peaks were attributed to the C-H bending and C=O stretching vibrations [31]. The appearance of these characteristic

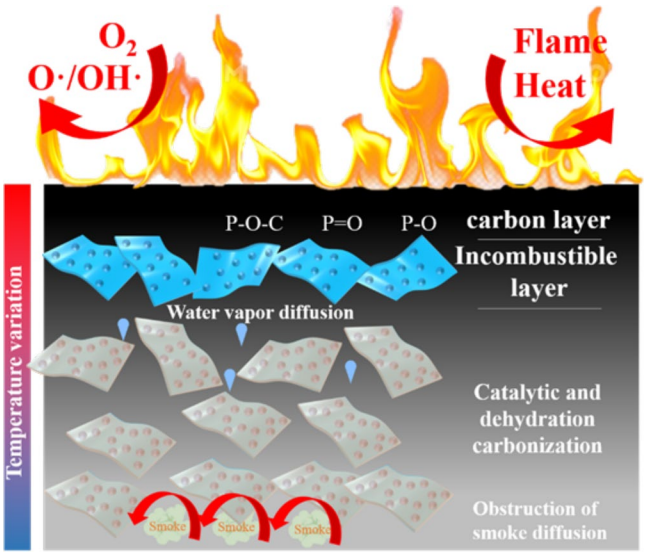

Fig. 7 (Color online) Schematic of the synergistic flame retarded mechanism for EVA/MXene @ Ag@PA composites

peaks may be attributed to the excellent catalytic effect of MXene@Ag@PA hybrid material, which created a stable carbon layer structure and preserved more intact EVA molecular chains during the combustion process. Consequently, the intensities of the related characteristic peaks significantly increased.

3.5 Possible flame retardancy mechanisms

Figure 7 illustrates the mechanism analysis of the potential flame-retardant effect of the MXene@Ag@PA hybrid material during the combustion of EVA composite materials. As evident, during combustion, the outer layer of MXene@Ag@PA hybrid material encapsulated PA, which decomposed to produce phosphoric acid and pyrophosphoric acid. These substances promoted the dehydration carbonization of organic materials in the EVA composite materials. Moreover, the moisture released from organic materials during dehydration absorbs heat and generates water vapor, thereby diluting flammable gases in the surrounding environment. Consequently, the residual material after carbonization formed a relatively stable carbon layer structure (containing P-O, P=O, and P-O-C), which prevented the penetration of flames and flammable gases from the outside and caused the decomposition of internal flammable materials [40]. Interestingly, MXene in the MXene@Ag@PA hybrid material could also act as a two-dimensional physical barrier, further enhancing the density of the carbon layer and increasing its flame resistance. In addition, the Ag nanoparticles in the MXene@Ag@PA hybrid material, along with the TiO_2 produced by MXene pyrolysis, accelerated the formation of the carbon layer. Therefore, both materials possessed catalytic carbonization capabilities, which contributed to condensed-phase flame retardation [41, 42].

4 Conclusion

This study successfully synthesized a MXene@Ag hybrid material surface coated with PA through a novel approach involving radiation modification and complexation reactions. This composite material significantly enhanced various key properties of EVA materials, including the mechanical performance, thermal conductivity, flame resistance, and electromagnetic wave shielding. Experimental data demonstrated that the addition of 2 parts of MXene@Ag@PA hybrid material could increase the thermal conductivity of the EVA composite materials by 44.2% . In terms of flame resistance, the introduction of MXene@Ag@PA hybrid material effectively reduced the peak heat release rate (pHRR), with a 30.1% decrease observed when two parts of MXene@Ag@PA hybrid material were added. Furthermore, post-combustion smoke production was significantly reduced, with a 28.3% decrease in the total smoke production (TSP), while the residual content increased to 19.1% . Notably, the electromagnetic shielding performance of the EVA composite materials was significantly enhanced, particularly in the X-band, where the electromagnetic interference shielding effectiveness (SET) can exceed 20 dB. In addition, the MXene@Ag@PA hybrid material could serve as a novel sensitizer for the radiation cross-linking of EVA, thereby improving the mechanical properties of the EVA composite materials following radiation exposure.

Author Contributions All authors contributed to the study conception and design. Material preparation, data collection, and analysis were performed by Si-Yi Xu and Lin-Fan Li. The first draft of the manuscript was written by Si-Yi Xu, and all authors commented on previous versions of the manuscript. All the authors have read and approved the final version of the manuscript.

Data availability The data that support the findings of this study are openly available in Science Data Bank at https://cstr.cn/31253.11.sciencedb.j00186.00360 and https://doi.org/10.57760/sciencedb.j00186.00360.

Declarations

Conflict of interest There are no conflict of interest to declare.

References

1. S. Pradhan, L. Unnikrishnan, S. Mohanty et al., Thermally conducting polymer composites with EMI shielding: a review. J. Electron. Mater. **49**, 1749–1764 (2020). https://doi.org/10.1007/s11664-019-07908-x
2. J. Sun, D. Zhou, Advances in graphene-polymer nanocomposite foams for electromagnetic interference shielding. Polym. **15**, 3235 (2023). https://doi.org/10.3390/polym15153235
3. M. Kim, H. Kim, S. Byun et al., PET fabric/polypyrrole composite with high electrical conductivity for EMI shielding. Synthetic Met. **126**, 233–239 (2002). https://doi.org/10.1016/S0379-6779(01)00562-8
4. D. Silva, P.J.M. Monteiro, Hydration evolution of C3S-EVA composites analyzed by soft X-ray microscopy. Cem. Concr. Res. **35**, 351–357 (2005). https://doi.org/10.1016/j.cemconres.2004.05.049
5. S. Liu, S. Zhou, A. Peng et al., Investigation of physiochemical and rheological properties of waste cooking oil/SBS/EVA composite modified petroleum asphalt. J. Appl. Polym. Sci. **137**, 48828 (2020). https://doi.org/10.1002/app.48828
6. H. Di, C. Deng, R.-M. Li et al., A novel EVA composite with simultaneous flame retardation and ceramifiable capacity. RSC Adv. **5**, 51248–51257 (2015). https://doi.org/10.1039/C5RA05781G
7. L. Lin, W. Wang, D. Li et al., Multifunctional graphene/Ag hydrogel with antimicrobial and catalytic properties for efficient solar-driven desalination and wastewater purification. Chem. Eng. J. **478**, 147249 (2023). https://doi.org/10.1016/j.cej.2023.147249
8. R. Verma, P. Thakur, A. Chauhan et al., A review on MXene and its' composites for electromagnetic interference (EMI) shielding applications. Carbon **208**, 170–190 (2023). https://doi.org/10.1016/j.carbon.2023.03.050
9. F. Shahzad, M. Alhabeb, C.B. Hatter et al., Electromagnetic interference shielding with 2D transition metal carbides (MXenes). Science **353**, 1137–1140 (2016). https://doi.org/10.1126/science.aag2421
10. W. Wang, Q. Liu, Y. Sun et al., Radiation polymerization for the preparation of universal coatings: remarkable anti-fogging and frost-resisting performance. RSC Adv. **14**, 10131–10145 (2024). https://doi.org/10.1039/d3ra08542b
11. F. Han, W. Wang, D. Li et al., Preparation of antibacterial nonwoven AgNCs@PP-g-PAA via radiation method. Nucl. Sci. Tech. **34**, 132 (2023). https://doi.org/10.1007/s41365-023-01292-2
12. M. Liu, K. Chen, Y. Shi et al., High-performance flexible nanocomposites with superior fire safety and ultra-efficient electromagnetic interference shielding. J. Mater. Sci. Technol. **166**, 133–144 (2023). https://doi.org/10.1016/j.jmst.2023.05.017
13. B. Yu, A.C.Y. Yuen, X. Xu et al., Engineering MXene surface with POSS for reducing fire hazards of polystyrene with enhanced thermal stability. J. Hazard. Mater. **401**, 123342 (2021). https://doi.org/10.1016/j.jhazmat.2020.123342
14. A. Ashfaq, M.-C. Clochard, X. Coqueret et al., Polymerization reactions and modifications of polymers by ionizing radiation. Polymers-basel. **12**, 2877 (2020). https://doi.org/10.3390/polym12122877
15. D. MacMartin, D. Visioni, B. Kravitz et al., Scenarios for modeling solar radiation modification. Proc. Natl. Acad. Sci. **119**, e2202230119 (2022). https://doi.org/10.1073/pnas.2202230119
16. S.K. Jaganathan, A. Balaji, M.V. Vellayappan et al., Radiation-induced surface modification of polymers for biomaterial application. J. Mater. Sci. **50**, 2007–2018 (2015). https://doi.org/10.1007/s10853-014-8718-x
17. V.Y. Kabanov, V.N.J.H.E.C. Kudryavtsev, Modification of polymers by radiation graft polymerization (State of the Art and Trends). High Energ. Chem. **37**, 1–5 (2003). https://doi.org/10.1023/A:1021919224451
18. F. Han, W.-R. Wang, D.-Y. Li et al., Simple synthesis of silver nanocluster composites AgNCs@PE-g-PAA by irradiation method and fluorescence detection of Cr^{3+}. Nucl. Sci. Tech. **34**, 73 (2023). https://doi.org/10.1007/s41365-023-01224-0
19. W. Cai, Z. Li, T. Cui et al., Self-assembly of hierarchical MXene@SnO_2 nanostructure for enhancing the flame retardancy, solar de-icing, and mechanical property of polyurethane resin. Compos. Pt. B-Eng. **244**, 110204 (2022). https://doi.org/10.1016/j.compositesb.2022.110204
20. X.-W. Cheng, J.-P. Guan, R.-C. Tang et al., Phytic acid as a bio-based phosphorus flame retardant for poly(lactic acid) nonwoven fabric. J. Clean. Prod. **124**, 114–119 (2016). https://doi.org/10.1016/j.jclepro.2016.02.113
21. Q. Chen, Z. Rong, Z. Liu et al., Application of modified phytic acid as flame retardant in cellulosic paper. Bioresource. **16**, 7953–7965 (2021). https://doi.org/10.15376/biores.16.4.7953-7965
22. Y. Zhou, M. Liu, Y. Wang et al., Significance of constructed MXene@Ag hybrids for enhancing the mechanical and tribological performance of epoxy composites. Tribol. Int. **165**, 107328 (2022). https://doi.org/10.1016/j.triboint.2021.107328
23. X. Jin, J. Wang, L. Dai et al., Flame-retardant poly(vinyl alcohol)/MXene multilayered films with outstanding electromagnetic interference shielding and thermal conductive performances. Chem. Eng. J. **380**, 122475 (2020). https://doi.org/10.1016/j.cej.2019.122475
24. H. Jiang, Y. Xie, R. Zhu et al., Construction of polyphosphazene-functionalized $Ti_3C_2T_X$ with high efficient flame retardancy for epoxy and its synergetic mechanisms. Chem. Eng. J. **456**, 141049 (2023). https://doi.org/10.1016/j.cej.2022.141049
25. T. Xu, D. Qian, Y. Hu et al., Assembled hybrid films based on sepiolite, phytic acid, polyaspartic acid and Fe^{3+} for flame-retardant cotton fabric. J. Polym. Eng. **42**, 744–754 (2022). https://doi.org/10.1515/polyeng-2022-0009
26. F. Wu, J. Xu, X. Qiu et al., Super-low-addition biobased flame retardant dedicated to polylactic acid through ionic reaction between phytic acid and taurine. Acs Appl. Polym. Mater. **3**, 4579–4586 (2021). https://doi.org/10.1021/acsapm.1c00671
27. S. Thota, V. Somisetti, S. Kulkarni et al., Covalent functionalization of cellulose in cotton and a nylon-cotton blend with phytic acid for flame retardant properties. Cellulose **27**, 11–24 (2020). https://doi.org/10.1007/s10570-019-02801-6
28. F. Song, T. Liu, Q. Fan et al., Sustainable, high-performance, flame-retardant waterborne wood coatings via phytic acid based green curing agent for melamine-urea-formaldehyde resin. Prog. Org. Coat. **162**, 106597 (2022). https://doi.org/10.1016/j.porgcoat.2021.106597
29. A. Patra, S. Kjellin, A.-C. Larsson, Phytic acid-based flame retardants for cotton. Green Mater. **8**, 123–130 (2020). https://doi.org/10.1680/jgrma.19.00054
30. X. Cheng, J.-P. Guan, X.-H. Yang et al., A bio-resourced phytic acid/chitosan polyelectrolyte complex for the flame retardant treatment of wool fabric. J. Clean. Prod. **223**, 342–349 (2019). https://doi.org/10.1016/j.jclepro.2019.03.157

31. K. Chen, M. Liu, Y. Shi et al., Multi-hierarchical flexible composites towards superior fire safety and electromagnetic interference shielding. Nano Res. **15**, 9531–9543 (2022). https://doi.org/10.1007/s12274-022-4883-6
32. H. Wang, K. Chen, Y. Shi et al., Flame retardant and multifunctional BC/MXene/MSiCnw/FRTPU aerogel composites with superior electromagnetic interference shielding via "Consolidating'' method. Chem. Eng. J. **474**, 145904 (2023). https://doi.org/10.1016/j.cej.2023.145904
33. L. Liu, J.B. Feng, Y.J. Xue et al., 2D MXenes for fire retardancy and fire-warning applications: promises and prospects. Adv. Funct. Mater. **33**, 2212124 (2023). https://doi.org/10.1002/adfm.202212124
34. H. Wu, S. Qiu, Y. Zhou et al., A novel carbon fiber/MXene coalition prepared by a bidirectional diazotization strategy: properties and applications. Colloid Surf. A. **642**, 128649 (2022). https://doi.org/10.1016/j.colsurfa.2022.128649
35. M. Mao, K. Yu, C. Cao et al., Facile and green fabrication of flame-retardant Ti3C2Tx MXene networks for ultrafast, reusable and weather-resistant fire warning. Chem. Eng. J. **427**, 131615 (2022). https://doi.org/10.1016/j.cej.2021.131615
36. M. Wan, C. Shi, X. Qian et al., Metal-organic framework ZIF-67 functionalized MXene for enhancing the fire safety of thermoplastic polyurethanes. Nanomaterials-Basel. **12**, 1142 (2022). https://doi.org/10.3390/nano12071142
37. Z. Wu, X. Feng, Y. Qu et al., Silane modified MXene/polybenzazole nanocomposite aerogels with exceptional surface hydrophobicity, flame retardance and thermal insulation. Compos. Commun. **37**, 101402 (2023). https://doi.org/10.1016/j.coco.2022.101402
38. Y. Li, Y. Zhu, S. Vallem et al., Flame-retardant ammonium polyphosphate/MXene decorated carbon foam materials as polysulfide traps for fire-safe and stable lithium-sulfur batteries. J. Energy Chem. **89**, 313–323 (2024). https://doi.org/10.1016/j.jechem.2023.10.029
39. H. Chen, Y. Li, P. Wang et al., Facile fabrication of low-content surface-assembled MXene in silicone rubber foam materials with lightweight, wide-temperature mechanical flexibility, improved flame resistance and exceptional smoke suppression. Compos. Part A: Appl. S. **177**, 107907 (2024). https://doi.org/10.1016/j.compositesa.2023.107907
40. H. Wang, Y. Jiang, Z. Ma et al., Hyperelastic, robust, fire-safe multifunctional MXene aerogels with unprecedented electromagnetic interference shielding efficiency. Adv. Funct. Mater. **33**, 2306884 (2023). https://doi.org/10.1002/adfm.202306884
41. Y. Luo, Y. Xie, H. Jiang et al., Flame-retardant and form-stable phase change composites based on MXene with high thermostability and thermal conductivity for thermal energy storage. Chem. Eng. J. **420**, 130466 (2021). https://doi.org/10.1016/j.cej.2021.130466
42. H. Chen, Z. Chen, M. Mao et al., Self-adhesive polydimethylsiloxane foam materials decorated with MXene/cellulose nanofiber interconnected network for versatile functionalities. Adv. Funct. Mater. **33**, 2304927(2023). https://doi.org/10.1002/adfm.202304927